




OPEN The dynamics of stomatal closure of *Arabidopsis thaliana* determined by terahertz spectroscopy and a water transport model

Jochen Taiber¹ , Jan Helminiak¹, Goretti G. Hernandez-Cardoso¹, Cornelius Mach¹, Alexander Jäckel¹, Oscar A. Naranjo-Montoya³, Enrique Castro-Camus^{1,3}, Peter Ache², Rainer Hedrich² & Martin Koch¹

Terahertz (THz) time-domain spectroscopy allows the detection of temporal changes of plant water content in vivo and non-destructively, for example over the course of the day or at the onset of drought stress. By studying a wildtype and a genetically modified variant of *Arabidopsis thaliana*, we observed significant differences in their dehydration dynamics. For a better understanding of the underlying processes, we modelled this behaviour with a simple rate equation model, compared the results with the experimental data and correlated our model with the biological regulatory mechanisms. In particular, under drought stress, we found an almost three times (2.80 ± 0.51) higher maximal stomatal opening in the mutant than in the wildtype. Over the course of the day, the degree of stomatal opening shows an exponential decrease with a half-life $t_{1/2}$ of 12.3 ± 2.6 h in the wildtype and 3.4 ± 0.8 h in the mutant.

Keywords Terahertz, Drought stress, *Arabidopsis thaliana*, Stomata

The development of stomata and stomatal control was a decisive step in the evolution of plants: Being able to dynamically adjust the opening state and thus the permeability of the epidermis makes it possible to adapt the water transport within the plant¹. In this way, vascular plants were able to colonise a wide variety of habitats with the most diverse conditions².

Under ideal irrigation conditions, the plant opens its stomata during daylight in order to be able to take up CO₂ for fixation via photosynthesis^{3–5}. However, stomatal opening is associated with water loss due to the exchange of water vapour. Closing of stomata reduces leaf evaporation and enables survival under extended drought periods, although photosynthesis is limited under these conditions. The underlying regulatory process is based on a complex biochemical signalling chain.

In general, water transport in plants takes place unidirectionally from the soil to the roots and then to the leaves. Here, the water is released into the environment as water vapour via the stomata. About 97% of the water uptaken is lost through transpiration and not used for growth or biochemical processes⁶. The driving force for this movement is the water potential, which under normal conditions decreases constantly from the soil to the stomata and the surrounding atmosphere^{6,7}. The water release is thus strictly controlled by the opening width of the stomatal pores.

Under drought conditions, the hormone abscisic acid (ABA) is synthesized, which initiates stomatal closure. In this process, ABA binds to a receptor that inactivates a PP2C-type phosphatase, which prevents the autophosphorylation of the protein kinase OST1 and other kinases. Phosphorylated OST1 can in turn phosphorylate the anion channel SLAC1 and thus activate it⁸. This is the initial step for an ion and water transport chain that leads to a volume decrease of the guard cells and finally results in stomatal closure⁹.

The opening state of the stomata in turn has a direct influence on the amount of water inside the plant leaf. Due to the fact that electromagnetic radiation in the THz range is strongly absorbed by water, THz spectroscopy is a very sensitive technique to measure changes in the water content of plants as shown in previous publications^{10–16}. An advantage of THz spectroscopy over conventional methods, such as gravimetry^{17,18} or

¹Faculty of Physics and Material Sciences Center, Philipps-Universität Marburg, Renthof 5, 35032 Marburg, Germany. ²Julius-von-Sachs-Institut für Biowissenschaften, Universität Würzburg, 97082 Würzburg, Germany. ³Centro de Investigaciones en Optica A.C., Loma del Bosque 115, Lomas del Campestre, 37150 Leon, Guanajuato, Mexico. ✉email: jochen.taiber@physik.uni-marburg.de

osmotic potential measurements^{19,20}, is that measurements can be performed *in vivo*, non-destructively and in a completely contactless fashion such that the plant remains unperturbed during the entire measurement period. It is also a direct measurement method, as the measured signal depends on the number of water molecules in the beam path eliminating the need for debatable assumptions. This makes this technique particularly suitable for time-resolved studies of the regulatory behaviour of the water balance of plants¹².

In our experiments, we compare the dehydration of wildtype *Arabidopsis thaliana* (Ler) and a mutant with defective protein kinase OST1, in other words, with defective stomatal response to drought stress (*ost1-2*,²¹). We present the first study including 20 plants in which the entire in-vivo water dynamics is monitored with minimal disturbance of the plants during the study. In addition, we model the drying process: First, we set up a water transport model based on biological process assumptions. We then select the relevant parameters including their time dependence describing the observed dynamics and vary them so that a good agreement between the model and each measurement is achieved. Finally, we interpret the obtained results in terms of their biological meaning.

Results

Comparison of wildtype and mutant drying behaviour using THz spectroscopy

To motivate the following discussion, we present two exemplary measurement curves of the drying process of *Arabidopsis thaliana*, one for the wildtype (Fig. 1a) and one for the *ost1-2* mutant with a defective stomatal regulatory mechanism (Fig. 1b). Irrigation was stopped at time $t = -2.5$ d. The ideal water status corresponds to the initial value of 80–85 wt%. The plots show that the wildtype can maintain this water level longer than the mutant. The time at which the water level is significantly reduced for the first time, starts three days earlier for the mutant. In the first night after this first water reduction, both wildtype and mutant can recover completely. After that, which is marked here with ❶, no complete recovery to the initial value can be observed for both plant types. Instead, wildtype and mutant lose water significantly thereafter, especially under illumination. After the water content has dropped below an average threshold of about 50 wt% (time ❷), no more water accumulation over the dark periods takes place. The leaf dries out completely within less than 24 hours. As a result of the earlier onset of desiccation in the mutant, the final state, i.e. complete drying of the measured plant leaf, also occurs earlier in the mutant than in the wildtype.

Particularly interesting, however, is the different behavior during the drying phase. For both plant types, the water loss is more severe in the illuminated periods than under non-illuminated conditions. In the mutant, however, this behavior is much more pronounced: Especially with illumination, the plant evaporates water to a large extent. These strong “day-night oscillations” were clearly visible in all *ost1-2* mutant plants measured which excludes random causes.

Modelling the drying process

For a better understanding of the underlying regulatory processes and to better quantify them, we present a compartmental model to describe the drying phase of a plant. First, we assume that the water in the sample system can be situated in two locations: in the soil and in the leaves. The water content A_s of the soil in the pot and the water content A_l of the leaves can be changed by two different processes each, which are characterized by water transfer rates (see Fig. 2).

The water transfer from the soil to the leaf is assumed to be proportional to the water content gradient, which is the difference of water content between the soil and the plant. The leaf gains water by drawing it from the soil at a rate of $k_1 \cdot (A_s - A_l)$. On the other hand, it loses water through evaporation from the stomata which happens at a rate $k_2 \cdot A_l$. Likewise, the soil loses water by direct evaporation at a rate $-k_3 \cdot A_s$. By combining all these loss and gain rates, we can construct the following system of differential equations

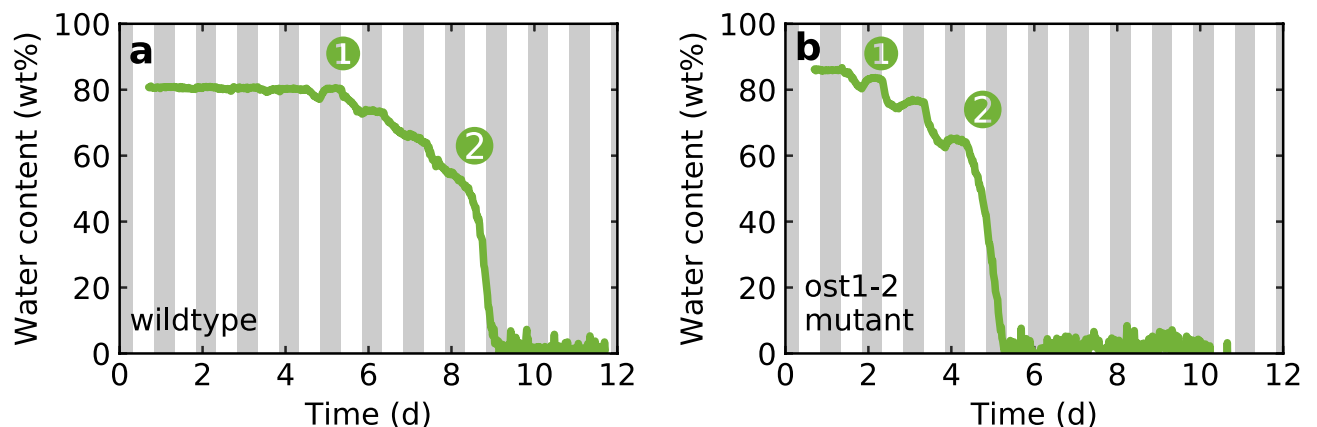


Fig. 1. Drying process of (a) wildtype and (b) *ost1-2* mutant of *Arabidopsis thaliana*. We show the water content over a period of 11 days. The white background indicates the illuminated periods (12 h), the grey background the non-illuminated periods (12 h).

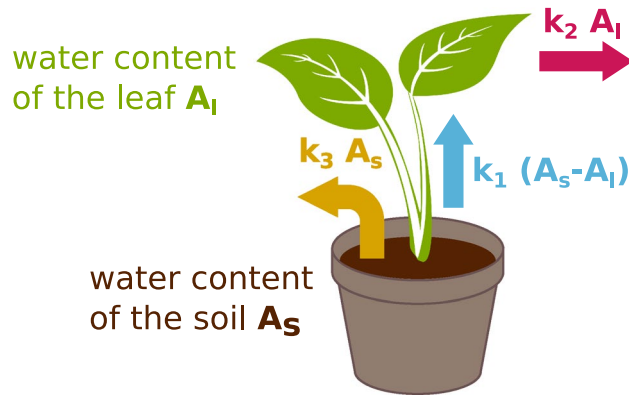


Fig. 2. Modelling parameters: water contents A_l and A_s and water transfer rates with weighting factors k_1 , k_2 and k_3 .

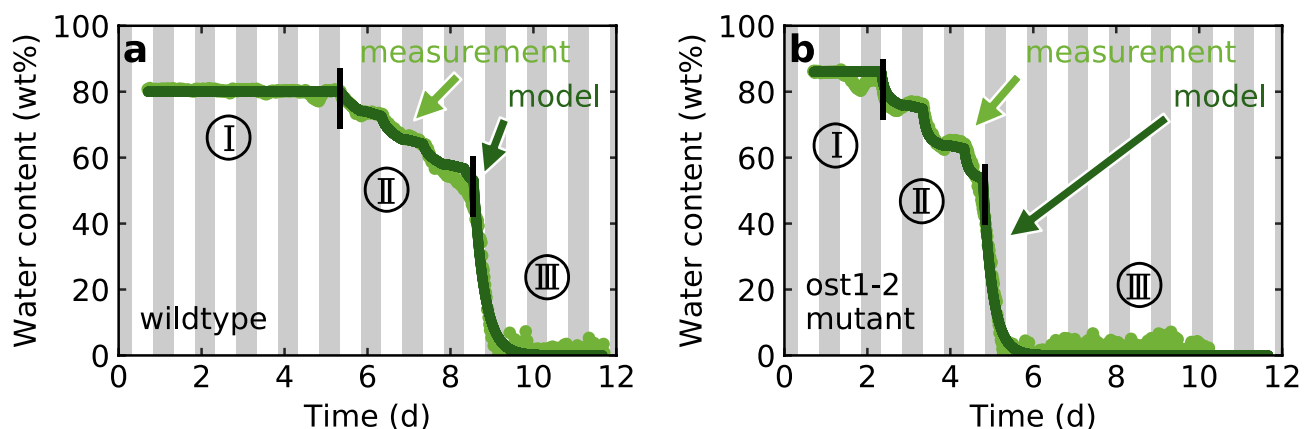


Fig. 3. Modelling results (dark green) for the drying process of (a) wildtype and (b) *ost1-2* mutant of *Arabidopsis thaliana*. The measured values are shown in light green.

The time-dependent factors k_i weight the corresponding rates: The factor k_1 modulates the water transfer from the soil to the plant leaf. The factor k_2 weights the water loss from the leaves, in other words, it represents the transconductance. Additionally, water evaporates from the soil for which the weighting factor k_3 is used. With this set of differential equations, the water dynamics of the plant-soil-system are modelled and the resulting solution is used to fit the experimental data. The results for exemplary drying phases of the wildtype and the *ost1-2* mutant of *Arabidopsis thaliana* are shown in Fig. 3. Here one can see that our model is able to describe the drying process qualitatively well in all temporal phases. Each fit parameter will be explained in the following paragraphs.

$$\frac{dA_l}{dt} = k_1 \cdot (A_s - A_l) - k_2 \cdot A_l, \quad (1)$$

$$\frac{dA_s}{dt} = -k_1 \cdot (A_s - A_l) - k_3 \cdot A_s. \quad (2)$$

The factor k_1 is mainly dominated by a step-function-like water transfer at the onset of drought stress. The full time course is shown in Fig. 4. In detail, it can be explained as follows: First, the plant maintains its optimum water content despite water loss through evaporation by drawing water from the soil (until ●) against a constant resistance. k_1 results from the differential equation 1 in the equilibrium state

$$k_1 = k_2 \cdot \frac{A_l}{A_s - A_l}. \quad (3)$$

However, this resistance is decisive for the relevant phase II (see Fig. 3), because it determines the maximum possible water transfer, characterised by $k_{1,\max}$. It is due to the retention of the soil and results physically from gravity, adhesion and cohesion. The equality of this value for both the wildtype and the mutant confirms that there is no difference in water transfer between roots and leaves.

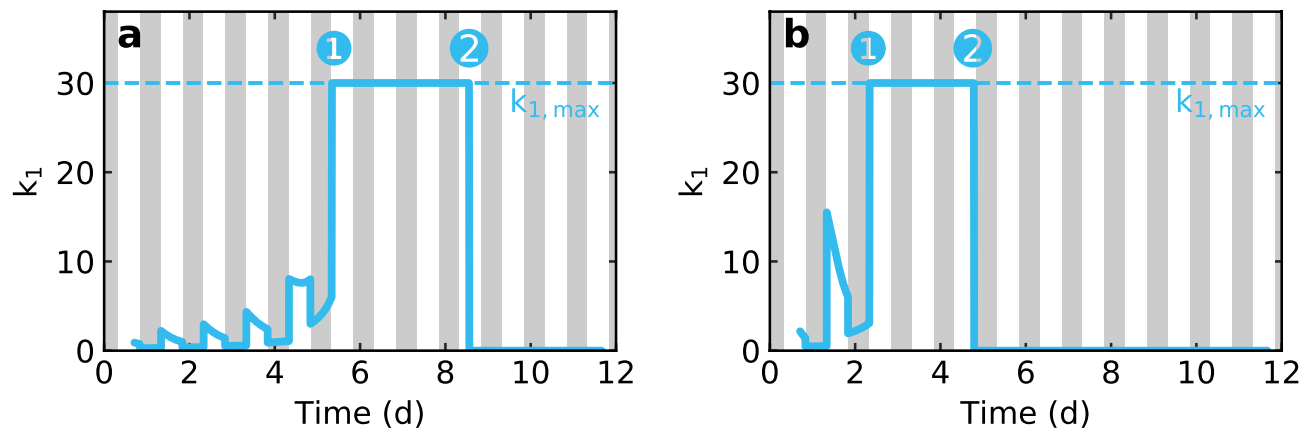


Fig. 4. Modelling results for the weighting factor k_1 in the drying process of *Arabidopsis thaliana*. As long as the plant can maintain its optimum water content, the time course of k_1 is determined by the evaporation of the plant. However, if this is no longer the case due to the decreasing soil water content, k_1 reaches its maximum value $k_{1,max}$ (●). This is identical for both the wildtype (a) and the mutant (b), which shows that the mutation does not cause any change in the processes that are decisive for the water transfer between roots and leaves. If the water potential of the soil falls below the critical threshold (permanent wilting point ⊙), the plant can no longer take up water and k_1 drops to zero. In the wildtype, this happens at a later point in time than in the mutant, but at the identical water potential of the soil.

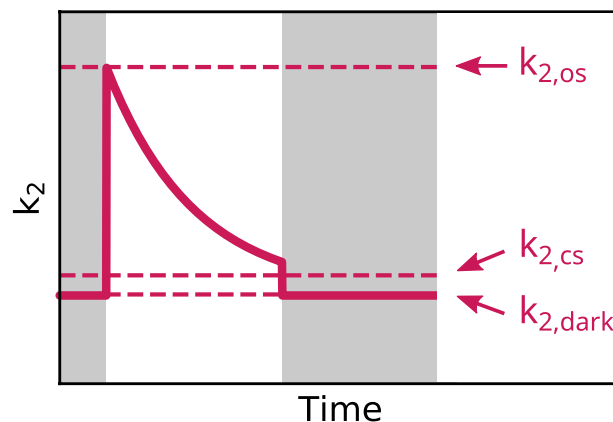


Fig. 5. Definition of $k_2(t)$ by parameters.

If the permanent wilting point is reached (⊙), which means that the water potential of the soil falls below a critical threshold, a regular water supply is no longer possible^{22–25}. This interruption of the transpirational pull happens within a very short time period, which justifies the assumption of a step-like function of k_1 . It is important here that the described threshold is identical for wildtype and mutant and occurs at the identical soil moisture content which is proved by gravimetric measurements.

For the factor k_3 , which determines the evaporation rate from the soil into the air, we assume a constant value that is independent of the illumination, in order to reduce the number of fit parameters and to obtain a model that is as simple as possible. This assumption has also been experimentally verified by carrying out gravimetric comparative experiments (see Supplementary Fig. S5 online). In these experiments the evaporation from the soil without plants over several lighting cycles was measured. The very minor differences that occur can be justified by the very small soil surface of the pots that we used exposed to light and air.

The parameter k_2 , which describes the transconductance, must show a clearly different dynamics for the wildtype and the mutant, revealing the defective regulatory pathway in the latter. Both plants open their stomata upon exposure to light (light-induced pathway)²¹, resulting in a large increase of leaf vapour exchange (see Fig. 5). Under drought stress, the plant now begins to close its stomata in order to reduce the water loss through evaporation.

Thus, we postulate that the parameter k_2 is described by an exponential decay during the bright periods

$$k_2(t) = (k_{2,os} - k_{2,cs}) e^{-t/\tau} + k_{2,cs} \quad (4)$$

and by a constant during the dark periods

$$k_2(t) = k_{2,\text{dark}} \quad (5)$$

This time dependency is determined by three fit parameters: The initial value $k_{2,\text{os}}$ with open stomata at the beginning of illumination, the value $k_{2,\text{dark}}$ without illumination and the time constant τ describing the exponential decay of the k_2 curve during the illumination phase. The final value $k_{2,\text{cs}}$ with closed stomata at the end of the illumination period is linked to $k_{2,\text{os}}$ via the constant factor $\Gamma_{\text{bright-dark}}$ comparing the bright and dark conditions

$$k_{2,\text{dark}} = \Gamma_{\text{bright-dark}} \cdot k_{2,\text{cs}} \quad (6)$$

which is determined empirically. This takes into account that the water loss with closed stomata is still higher in illuminated conditions than in non-illuminated which will be discussed in more detail later. The entire k_2 dynamics for both wildtype and *ost1-2* mutant are shown in Fig. 6.

In order to provide a solid basis for our assumption, we have tested various alternative functions for the progression of k_2 over time (see Supplementary Fig. S2 and S3 online), corresponding to different physiological explanations. Due to these tests, we are able to show that the measurement results are only approximated sufficiently well with the assumption of an exponential decay which is typical in nature. Furthermore, it should be noted that the behaviour described here is only valid in the phase of existing drought stress, in other words when the water supply from the soil is insufficient. With optimal water supply, the plant tries to keep the stomata open for as long as possible.

Figure 7a shows that the water loss at the beginning of the illumination period is significantly higher in the mutant than in the wildtype. However, the value drops to the same final level over the course of the day (Fig. 7b). The half-life $t_{1/2}$ (Fig. 7c) again shows a significant difference between wildtype and mutant which is probably also due to the higher degree of opening at the start of illumination. The ratio between $k_{2,\text{os}}$ and $k_{2,\text{cs}}$ therefore serves as a characteristic parameter for the influence of the regulatory mechanisms on the water balance of the plant.

A look at the statistical significance: The parameter $k_{2,\text{os}}$, indicating the maximum stomatal opening, differs significantly at the 0.01 level between wildtype and mutant. The same applies for the half-life $t_{1/2}$ of the exponential closure of the stomata, but no significant difference can be found for $k_{2,\text{cs}}$, which indicates the minimum stomatal opening during illumination.

Discussion

Our measurement technique provides a direct way to determine the hydration status of a plant over time without the need of fundamental assumptions, as is the case with indirect methods. Noteworthy is the detailed data set with 20 individual analyses. The behaviour described here can be seen in all measurement series carried out, which provides a solid basis for the conclusions drawn. By modelling the dehydration process, we improve the understanding of the plant mechanisms under drought stress. Our simple approach describes the experimental data very well, which indicates that transpiration is by far the dominant driving force for water uptake from the soil and transport. Further interactions between root/xylem and xylem/leaf are of course also of interest, but do not seem to play the major role in the net approach presented here. In detail: We can divide the drying process into three different phases:

- In the first phase (Fig. 3: phase I), the plant maintains its optimal water content in the leaves, although the water supply through the soil is already severely limited. This is only possible by active regulation of stomatal

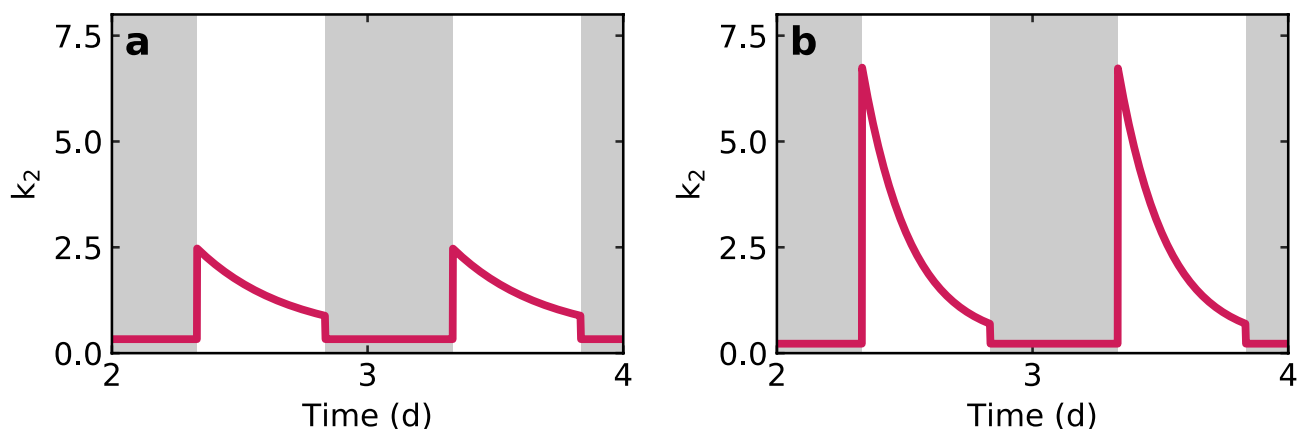


Fig. 6. Modelling results for the weighting factor k_2 , which describes the water loss of the leaf in the drying process of (a) wildtype and (b) *ost1-2* mutant of *Arabidopsis thaliana*. In the mutant, it reaches much higher values than in the wildtype.

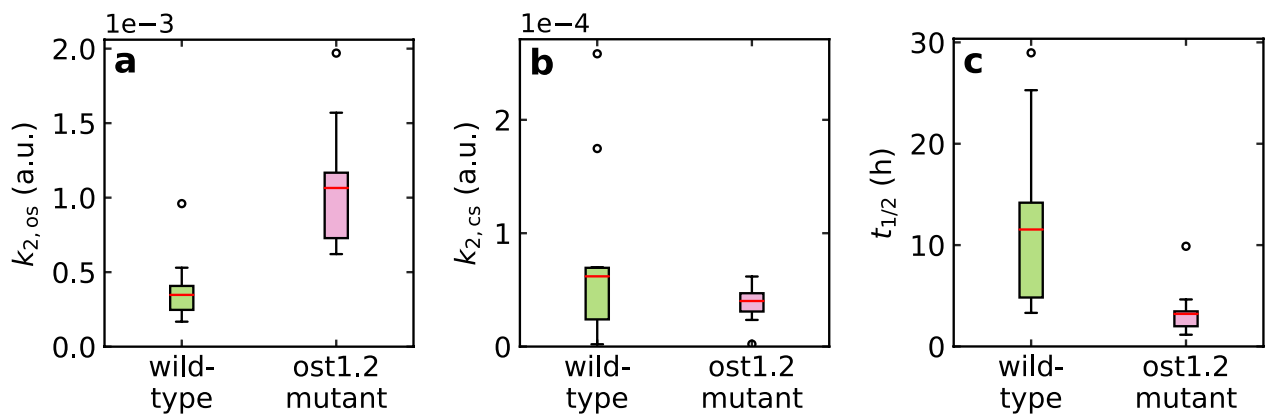


Fig. 7. Obtained fit parameters for 20 individual plants. **(a)** The $k_{2,os}$ value for the mutant, which determines the maximum stomatal opening, is significantly higher than for the wildtype. By contrast, the minimum stomatal opening during illumination, indicated by $k_{2,cs}$, shows similar values for both wildtype and mutant **(b)**. **(c)** The half-life $t_{1/2}$ for the exponential decrease in transpiration during the course of the day is higher for the wildtype than for the mutant (partly overlapping value ranges) which is also an effect of the rapid stomatal closure capability via the ABA signalling pathway.

opening and thus the gas exchange. It can be seen by the fact that this phase lasts only about four days in the *ost1-2* mutant, whereas the water content remains at the optimal level for about seven days in the wildtype, calculated from the stop of irrigation.

- In the second phase (Fig. 3: phase II), the plant starts losing water significantly as the water supply from the soil is very low due to decreasing water potential. As a result of the light induced stomatal opening, the water loss is higher during illumination than in non-illuminated periods and is significantly higher in the *ost1-2* mutant than in the wildtype due to the flawed stomatal closure. At the beginning of this phase, the water content increases again under non-illuminated conditions as a consequence of the lower evaporation and the still present water supply from the soil. This nighttime moisture recovery appears more pronounced in the mutant due to the higher water loss under illumination. But towards the end of the phase, this is no longer the case and the plant also loses water under non-illuminated conditions. These day-night-oscillations are the characteristic feature of the plant's dehydration behaviour.
- In the third phase (Fig. 3: phase III), the water transport to certain leaves is blocked. In addition to excessive soil water retention, further explanations include the occurrence of cavitation and embolisms^{26–28} after reaching the turgor loss point²⁹. The water loss in this phase is even higher than with fully opened stomata, which indicates structural damage in the plant. Abscission or apoptosis processes to stop water loss through the leaves and to protect roots and stem may also play a role^{6,30}.

Having a closer look at the modelling, the evolution of k_1 has to be mentioned. A good agreement with the results is obtained only by applying a discontinuous step (see Fig. 4a). It can not be obtained if the drop occurs softly over a longer period of time. As can be seen in Fig. 3, once the plant has fallen below a water content of about 50 wt%, the remaining water in the leaves rapidly decreases, much faster than could be explained by mere evaporation under unchanged conditions. This suggests that soil retention brings water uptake to an abrupt halt and supports the hypothesis of occurring embolisms or even apoptosis or abscission processes.

Regarding the stomatal behaviour: In the first two phases, there is a strong agreement between the model and the measured values if we assume an exponential decay for the water loss of the leaves with two different initial levels $k_{2,os}$, one for the wildtype and one for the mutant. The latter opens its stomata more strongly than the wildtype at the onset of illumination.

A key role is played by different rates of the processes that lead to stomatal closure. Interestingly, wildtype and mutant differ in the half-life $t_{1/2}$ of the exponential decrease in evaporation, which is 12.3 ± 2.6 h in the wildtype and 3.4 ± 0.8 h in the mutant. Both times are relatively long, which suggests that they do not describe a direct response to ABA production. The described ABA induced signaling via OST1 occurs on a very short time scale within several minutes and is not directly visible in the terahertz data as we measure the total water content in the leaf and not the inflow or outflow. Changes to these are accessible by turgor pressure measurements which the authors are showing in a different publication⁹. However, our focus in this study is on the change in water content in the leaf of the plant.

It is relevant to point out that in the *ost1-2* mutant, only the ABA induced signaling pathway via OST1 is disrupted. Stomatal regulation by light or CO_2 , for example, is largely unrestricted^{9,21}. In general: At the end of the non-illuminated period, the plant's energy stores are relatively empty. The main focus is therefore on obtaining energy through photosynthesis. In order to absorb as much CO_2 as possible, both *Arabidopsis* variants open their stomata at the abrupt onset of light as wide as possible, which is accompanied by increased water loss. During the course of the day, the stores, e.g. in the form of starch, are refilled and reducing the water loss is prioritised more strongly again. While the wildtype reacts to water shortage as a criterion for regulating its

water loss and prioritises this regulation, the mutant only follows pure energy demand management. This could explain the exponential course and the differences between wildtype and mutant. Dittrich et al.³¹ and Merilo et al.³² measured the gas exchange to show that deactivating the relevant ABA receptors has a significant influence on transpiration, but it is not exclusively dependent on these receptors and stomatal closure can still occur. A response to drought stress is, to a limited extent, therefore also possible via ABA independent pathways such as reduced hydraulic turgor pressure^{2,33,34} or low humidity^{31,32}. The latter presumably also plays a role in this experiment due to the relatively low air humidity values.

Having a look at Fig. 7, which shows the values for the fit parameters of all evaluated plants: Comparing the values of the parameter $k_{2,cs}$ that describes the minimum water loss from the leaf under illumination, no significant difference can be found. This allows the conclusion that the mutation does not influence the minimum evaporation when the stomata are closed.

The influence of the mutation, however, is visible in the strongly differing maximum degree of stomatal opening and shows the intact or impaired regulation of the stomatal opening via the ABA pathway. It also seems likely that the wildtype does not fully open its stomata in acute drought stress which is another reason for the lower initial level of stomata opening at the beginning of the illumination. Our experiments even allow us to quantify the difference in the degree of opening: This is 2.80 ± 0.51 times higher in the mutant than in the wildtype.

In order to achieve a good agreement between the model and the measured data, it is necessary that the water loss rate, determined by the parameter k_2 , is lower during non-illuminated conditions compared to illuminated conditions and closed stomata. This can be caused by incomplete closure, for example through restricted control of stomata that are still under development, or by water loss through other paths, such as cuticular transpiration or via hydathodes. This hypothesis is supported by the fact that the stomatal conductance is not zero even with closed stomata as already shown^{35–37}. In our study, we therefore introduced the factor $\Gamma_{\text{bright} - \text{dark}}$ in Eq. (6) and determined it empirically by optimising the agreement of our model with the measurement data. This shows that by far the largest proportion of total water loss occurs through the open stomata, see also^{38–40}. Lawson and Cominelli, for example, both gives a portion of 95%^{36,41} which is in adequate good agreement with our empirically determined value of $\Gamma_{\text{bright} - \text{dark}}$ of 92%. Growing conditions also play a role: If these are optimal, i.e. if there is high humidity, insensitivity to ABA can occur resulting in reduced stomatal closure.

In addition to the fundamental findings on the drought stress response described above, we were able to reduce the different dynamics in the water balance between the wildtype and the *ost1-2* mutant to crucial parameters. A possible application for this could be in the field of phenotyping: Investigations using technologies in the terahertz range could provide an alternative method to thermal imaging in mutant screening, as proposed by Merlot et al.⁴². In this way, the influence of certain gene modifications on the water balance of the plant can be elucidated with high-precision measurements. Especially in view of longer periods of drought due to climate change, both a better understanding of the drought stress response and a tool that helps with developments in enhancing drought stress tolerance are eminently important.

Methods

Plant samples

Two variants of *Arabidopsis thaliana* were investigated: Landsberg erecta (Ler) as wildtype and *ost1-2* as mutant^{21,42} (photos are shown in Fig. S4 online). The plants were cultivated in the lab in tubes with 34.0 g soil each under fully controlled growing conditions: photoperiod of 12h with illumination by 85–95 $\mu\text{mol m}^{-2} \text{s}^{-1}$ white light (400 W, Bio Green Sirius X400), air-conditioner regulated temperature of 18 °, which rises to 20 ° when illuminated, and relative humidity of 32–45 %. For the measurements, care was taken to select plants with the most uniform leaf growth possible to avoid differences in water loss due to different leaf surface areas. To improve the statistics, three series of 15 plants each were recorded. The automatic fit procedure was performed for each individual plant. 20 fit results (10x wildtype, 10x mutant) with an R^2 value > 0.99 were then selected for further evaluation, see results in Fig. 7. This selection of the measurement series according to the goodness of fit was carried out because the automated fit procedure was not possible for all plants. Some plants died prematurely, but not from water stress, and do not reach the characteristic phase II of the day-night oscillations, while others show measurement errors due to insufficient fixation of the leaf. Our fit selection criterion therefore appears appropriate, as all plants with a normal drought stress phase are taken into account.

THz time-domain spectroscopy

All measurements were recorded using a THz time domain spectroscopy setup consisting of a 1550 nm fiber-coupled femtosecond laser (Menlo C-Fiber), a mechanical free space delay line and fibre-coupled photoconductive antennas (InGaAs/InAlAs multilayer structure). For long-term measurements of whole plant series, the system was fully automated, see Fig. 8: The antennas were mounted on a circularly moving arm of a goniometer, driven by a computer-controlled stepper motor to allow continuous measurements of 15 plants over a period of several weeks¹¹.

Measurements

All plants are arranged in the setup in such a way that one particular leaf is fixed by magnetic stripes and is thus available for transmission measurements. Over the entire duration of the experiment, each plant was always measured at the identical spot with a diameter of 3 mm at the mesophyll. Light conditions were 60–85 $\mu\text{mol m}^{-2} \text{s}^{-1}$ white light (400 W, Bio Green Sirius X400) with a photoperiod of 12h. Care was taken to touch or shade the sheet only at the outermost edge to minimize the influence of the fixation. Before the start of a measurement series, irrigation of the plants was stopped to create drought stress. Each measurement series was then carried out for 8 to 14 days until each plant was completely dried out, with a measurement signal recorded every 25 min

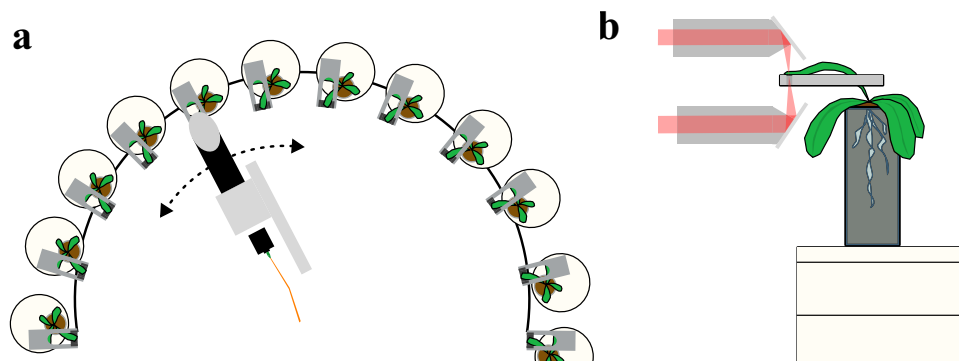


Fig. 8. (a) Circularly moving measurement head for automated measurements of 15 plants. (b) Side view: the transmission beam path through a plant leaf is shown in red. The plant is positioned on a scale for additional gravimetric data.

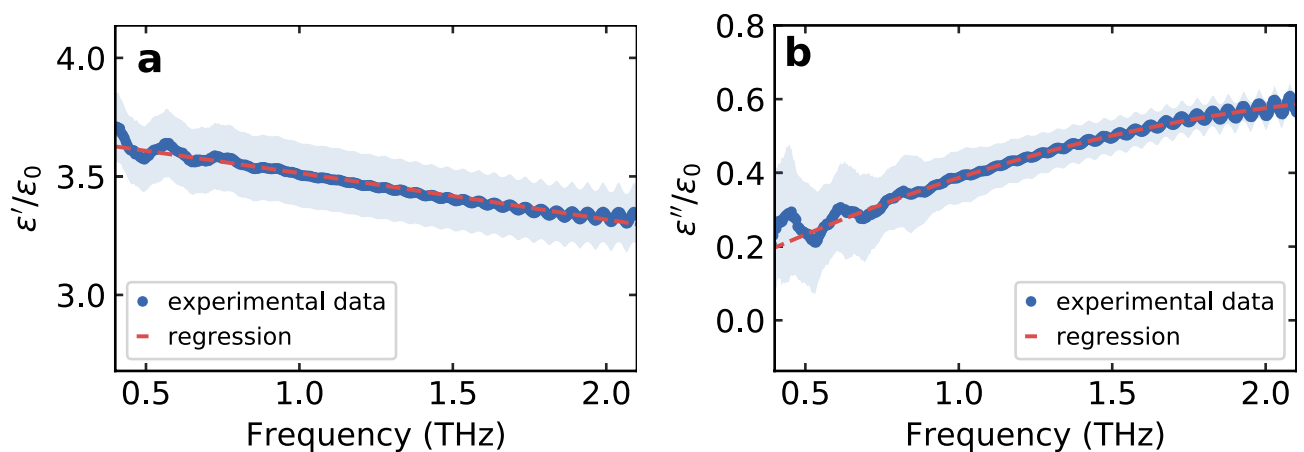


Fig. 9. (a) Real and (b) imaginary part of the dielectric function of dry material of *Arabidopsis thaliana* in the terahertz band.

for each individual plant. Immediately before each measurement of a plant leaf, a reference measurement is taken to remove the influence of system fluctuations or ambient conditions.

Signal processing (effective medium theory)

In each case, a complete THz time trace of 50 ps was recorded. By applying a Fourier transform, the signal is transferred into the frequency domain⁴³. The experimental transfer function is calculated by dividing the measured transmission signal by the corresponding reference signal.

To extract the water content of the leaf from the measured THz signal, we apply an effective medium theory: Here, the plant leaf is considered as an “effective medium”, thus a composition of various substances. Instead of considering the complex structure, the leaf is described by the dielectric properties and the relative fractions of its individual components. In our case, we assume that the plant leaf consists of the three components air, water and dry material and then apply the Landau-Lifschitz-Looyenga model to calculate the resulting dielectric function of the leaf^{43,44}

$$\sqrt[3]{\epsilon_{\text{res}}} = X_{\text{water}} \cdot \sqrt[3]{\epsilon_{\text{water}}} + X_{\text{dry material}} \cdot \sqrt[3]{\epsilon_{\text{dry material}}} + X_{\text{air}} \cdot \sqrt[3]{\epsilon_{\text{air}}}. \quad (7)$$

The dielectric function of water is approximated by the Double Debye model^{45,46}, while that of the dry material is determined experimentally. To do this, the leaves of the measured *Arabidopsis thaliana* plants were removed and dried. They were then ground to a fine powder using a mortar and compressed into a tablet using a hydraulic press (100 µg material with an applied force of 30 kN over a period of 90 s). Subsequently, these tablets were processed using a THz transmission setup (HHI TeraWave⁴⁷) under nitrogen atmosphere to avoid any influence of atmospheric water. The resulting dielectric function can be seen in Fig. 9 and can be fitted with f as the frequency in terahertz by

$$\epsilon' = -0.01 \text{ THz}^{-2} \epsilon_0 f^2 - 0.18 \text{ THz}^{-1} \epsilon_0 f + 3.7 \epsilon_0 \text{ and } \epsilon'' = -0.08 \text{ THz}^{-2} \epsilon_0 f^2 + 0.43 \text{ THz}^{-1} \epsilon_0 f + 0.04 \epsilon_0. \quad (8)$$

Using Eq. 7, the theoretical transfer function can be calculated as explained in¹³. Then this is fitted to the experimentally obtained transfer function within the range from 0.1 to 0.3 THz, using the water content as the fit parameter X_{water} and assuming a fixed ratio between $X_{\text{dry material}}$ and X_{air} which was experimentally justified. It should be noted that the thickness of the plant leaf also plays a role: Since this changes during the drying process, a minor linear correction of the thickness based on experimental data was implemented in the evaluation program. This was designed by a combination of exemplary thickness determination from the terahertz signal itself using Fabry-Perot pulses^{48,49} and mechanical measurements using a micrometer screw, as an individual correction is too unstable due to the inhomogeneity and complexity of a plant leaf. In this way, the relative water content of the plant leaf can be obtained from the measured THz time domain signals. More detailed information about the application of the effective medium theory to biological samples can be found in^{13,50–52}.

Supportive measurements

In order to quantify and to minimize the influence of the environment, the temperature, relative humidity, the amount of particulate matter and the CO₂ content of the atmosphere were permanently recorded. Individual scales for each plant, which are read out automatically, allow parallel recording of the weight changes and thus comparison with gravimetric data, which are in very good agreement with the THz data obtained.

Data availability

The data that support the findings of this study are available from the corresponding authors upon reasonable request. Requests should be addressed to J.T.

Received: 26 February 2025; Accepted: 12 September 2025

Published online: 23 September 2025

References

- Jones, H. G. & Sutherland, R. A. Stomatal control of xylem embolism. *Plant Cell Environ.* **14**, 607–612. <https://doi.org/10.1111/j.1365-3040.1991.tb01532.x> (1991).
- Brodribb, T. J. & McAdam, S. A. M. Passive origins of stomatal control in vascular plants. *Science (New York, N.Y.)* **331**, 582–585. <https://doi.org/10.1126/science.1197985> (2011).
- Ingenhousz, J. *Experiments Upon Vegetables, Discovering Their Great Power of Purifying the Common Air in the Sun-Shine, and of Injuring it in the Shade and at Night*. (Printed for P. Elmsly and and H. Payne, 1779).
- Clark, J. W. et al. The origin and evolution of stomata. *Curr. Biol. CB* **32**, R539–R553. <https://doi.org/10.1016/j.cub.2022.04.040> (2022).
- Hetherington, A. M. & Woodward, F. I. The role of stomata in sensing and driving environmental change. *Nature* **424**, 901–908. <https://doi.org/10.1038/nature01843> (2003).
- Taiz, L. *Plant Physiology and Development*. 6 Ed. (Sinauer, 2015).
- Steudle, E. The cohesion-tension mechanism and the acquisition of water by plant roots. *Annu. Rev. Plant Physiol. Plant Mol. Biol.* **52**, 847–875. <https://doi.org/10.1146/annurev.arplant.52.1.847> (2001).
- Roelfsema, M. R. G., Hedrich, R. & Geiger, D. Anion channels: Master switches of stress responses. *Trends Plant Sci.* **17**, 221–229. <https://doi.org/10.1016/j.tplants.2012.01.009> (2012).
- Ache, P. et al. Stomatal action directly feeds back on leaf turgor: new insights into the regulation of the plant water status from non-invasive pressure probe measurements. *Plant J. Cell Mol. Biol.* **62**, 1072–1082. <https://doi.org/10.1111/j.1365-3113.2010.04213.x> (2010).
- Mittleman, D. M., Jacobsen, R. H. & Nuss, M. C. T-ray imaging. *IEEE J. Sel. Top. Quantum Electron.* **2**, 679–692. <https://doi.org/10.1109/2944.571768> (1996).
- Born, N. et al. Monitoring plant drought stress response using terahertz time-domain spectroscopy. *Plant Physiol.* **164**, 1571–1577. <https://doi.org/10.1104/pp.113.233601> (2014).
- Castro-Camus, E., Palomar, M. & Covarrubias, A. A. Leaf water dynamics of *Arabidopsis thaliana* monitored in-vivo using terahertz time-domain spectroscopy. *Sci. Rep.* **3**, 2910. <https://doi.org/10.1038/srep02910> (2013).
- Gente, R. et al. Determination of leaf water content from terahertz time-domain spectroscopic data. *J. Infrared Millimeter Terahertz Waves* **34**, 316–323. <https://doi.org/10.1007/s10762-013-9972-8> (2013).
- Singh, A. K., Pérez-López, A. V., Simpson, J. & Castro-Camus, E. Three-dimensional water mapping of succulent *Agave victoriae-reginae* leaves by terahertz imaging. *Sci. Rep.* **10**, 1404. <https://doi.org/10.1038/s41598-020-58277-z> (2020).
- Pagano, M. et al. Thz water transmittance and leaf surface area: An effective nondestructive method for determining leaf water content. *Sensors (Basel, Switzerland)* **19**. <https://doi.org/10.3390/s19224838> (2019).
- Baldacci, L. et al. Non-invasive absolute measurement of leaf water content using terahertz quantum cascade lasers. *Plant Methods* **13**, 51. <https://doi.org/10.1186/s13007-017-0197-z> (2017).
- Garnier, E. & Laurent, G. Leaf anatomy, specific mass and water content in congeneric annual and perennial grass species. *New Phytol.* **128**, 725–736. <https://doi.org/10.1111/j.1469-8137.1994.tb04036.x> (1994).
- Ozeki, K., Miyazawa, Y. & Sugiura, D. Rapid stomatal closure contributes to higher water use efficiency in major c4 compared to c3 Poaceae crops. *Plant Physiol.* **189**, 188–203. <https://doi.org/10.1093/plphys/kiac040> (2022).
- Morgan, J. M. Osmoregulation and water stress in higher plants. *Annu. Rev. Plant Physiol.* **35**, 299–319. <https://doi.org/10.1146/annurev.pp.35.060184.001503> (1984).
- Sanders, G. J. & Arndt, S. K. Osmotic adjustment under drought conditions. In *Plant Responses to Drought Stress* (Aroca, R. Ed.). 199–229. https://doi.org/10.1007/978-3-642-32653-0_8 (Springer, 2012).
- Mustilli, A.-C., Merlot, S., Vavasseur, A., Fenzi, F. & Giraudat, J. *Arabidopsis* ost1 protein kinase mediates the regulation of stomatal aperture by abscisic acid and acts upstream of reactive oxygen species production. *Plant Cell* **14**, 3089–3099. <https://doi.org/10.1105/tpc.007906> (2002).
- Munné-Bosch, S. & Alegre, L. Die and let live: Leaf senescence contributes to plant survival under drought stress. *Funct. Plant Biol. FPB* **31**, 203–216. <https://doi.org/10.1071/FP03236> (2004).
- McDowell, N. et al. Mechanisms of plant survival and mortality during drought: Why do some plants survive while others succumb to drought? *New Phytol.* **178**, 719–739. <https://doi.org/10.1111/j.1469-8137.2008.02436.x> (2008).
- Johnson, D. M., Katul, G. & Domec, J.-C. Catastrophic hydraulic failure and tipping points in plants. *Plant Cell Environ.* **45**, 2231–2266. <https://doi.org/10.1111/pce.14327> (2022).

25. Trifilò, P., Abate, E., Petruzzellis, F., Azzarà, M. & Nardini, A. Critical water contents at leaf, stem and root level leading to irreversible drought-induced damage in two woody and one herbaceous species. *Plant Cell Environ.* **46**, 119–132. <https://doi.org/10.1111/pce.14469> (2023).
26. Cochard, H. Xylem embolism and drought-induced stomatal closure in maize. *Planta* **215**, 466–471. <https://doi.org/10.1007/s00425-002-0766-9> (2002).
27. Tyree, M. T. & Sperry, J. S. Vulnerability of xylem to cavitation and embolism. *Annu. Rev. Plant Physiol. Plant Mol. Biol.* **40**, 19–36. <https://doi.org/10.1146/annurev.pp.40.060189.000315> (1989).
28. Lens, F. et al. Embolism resistance as a key mechanism to understand adaptive plant strategies. *Curr. Opin. Plant Biol.* **16**, 287–292. <https://doi.org/10.1016/j.pbi.2013.02.005> (2013).
29. Scoffoni, C. et al. The causes of leaf hydraulic vulnerability and its influence on gas exchange in *Arabidopsis thaliana*. *Plant Physiol.* **178**, 1584–1601. <https://doi.org/10.1104/pp.18.00743> (2018).
30. González-Carranza, Z. H. et al. A novel approach to dissect the abscission process in *Arabidopsis*. *Plant Physiol.* **160**, 1342–1356. <https://doi.org/10.1104/pp.112.205955> (2012).
31. Dittrich, M. et al. The role of *Arabidopsis* aba receptors from the pyr/pyl/rcar family in stomatal acclimation and closure signal integration. *Nat. Plants* **5**, 1002–1011. <https://doi.org/10.1038/s41477-019-0490-0> (2019).
32. Merilo, E. et al. Pyr/rcar receptors contribute to ozone-, reduced air humidity-, darkness-, and CO₂-induced stomatal regulation. *Plant Physiol.* **162**, 1652–1668. <https://doi.org/10.1104/pp.113.220608> (2013).
33. Buckley, T. N. The control of stomata by water balance. *New Phytol.* **168**, 275–292. <https://doi.org/10.1111/j.1469-8137.2005.01543.x> (2005).
34. Tombesi, S. et al. Stomatal closure is induced by hydraulic signals and maintained by aba in drought-stressed grapevine. *Sci. Rep.* **5**, 12449. <https://doi.org/10.1038/srep12449> (2015).
35. Raschke, K. & Hedrich, R. Simultaneous and independent effects of abscisic acid on stomata and the photosynthetic apparatus in whole leaves. *Planta* **163**, 105–118. <https://doi.org/10.1007/BF00395904> (1985).
36. Lawson, T. & Matthews, J. Guard cell metabolism and stomatal function. *Annu. Rev. Plant Biol.* **71**, 273–302. <https://doi.org/10.1146/annurev-arplant-050718-100251> (2020).
37. Kadereit, J. W., Körner, C., Kost, B. & Sonnewald, U. *Strasburger—Lehrbuch der Pflanzenwissenschaften* (Springer, 2014).
38. Waggoner, P. E. & Zelitch, I. Transpiration and the stomata of leaves: Water loss through leaf pores is controlled by pore size, which varies with environment and chemical sprays. *Science* **150**, 1413–1420 (1965).
39. Cowan, I. R. & Troughton, J. H. The relative role of stomata in transpiration and assimilation. *Planta* **97**, 325–336. <https://doi.org/10.1007/BF00390212> (1971).
40. Boyer, J. S. Turgor and the transport of CO₂ and water across the cuticle (epidermis) of leaves. *J. Exp. Bot.* **66**, 2625–2633. <https://doi.org/10.1093/jxb/erv065> (2015).
41. Cominelli, E., Galbiati, M. & Tonelli, C. Transcription factors controlling stomatal movements and drought tolerance. *Transcription* **1**, 41–45. <https://doi.org/10.4161/trns.1.1.12064> (2010).
42. Merlot, S. et al. Use of infrared thermal imaging to isolate *Arabidopsis* mutants defective in stomatal regulation. *Plant J. Cell Mol. Biol.* **30**, 601–609. <https://doi.org/10.1046/j.1365-3113X.2002.01322.x> (2002).
43. Jepsen, P. U., Cooke, D. G. & Koch, M. Terahertz spectroscopy and imaging - Modern techniques and applications. *Laser Photon. Rev.* **5**, 124–166. <https://doi.org/10.1002/lpor.201000011> (2011).
44. Looyenga, H. Dielectric constants of heterogeneous mixtures. *Physica* **31**, 401–406. [https://doi.org/10.1016/0031-8914\(65\)90045-5](https://doi.org/10.1016/0031-8914(65)90045-5) (1965).
45. Liebe, H. J., Hufford, G. A. & Manabe, T. A model for the complex permittivity of water at frequencies below 1 THz. *Int. J. Infrared Millimeter Waves* **12**, 659–675. <https://doi.org/10.1007/BF01008897> (1991).
46. Rønne, C. et al. Investigation of the temperature dependence of dielectric relaxation in liquid water by THz reflection spectroscopy and molecular dynamics simulation. *J. Chem. Phys.* **107**, 5319–5331. <https://doi.org/10.1063/1.474242> (1997).
47. Vieweg, N. et al. Terahertz-time domain spectrometer with 90 db peak dynamic range. *J. Infrared Millimeter Terahertz Waves* **35**, 823–832. <https://doi.org/10.1007/s10762-014-0085-9> (2014).
48. Scheller, M., Jansen, C. & Koch, M. Analyzing sub-100-um samples with transmission terahertz time domain spectroscopy. *Opt. Commun.* **282**, 1304–1306. <https://doi.org/10.1016/j.optcom.2008.12.061> (2009).
49. Duvillaret, L., Garet, F. & Coutaz, J. L. Highly precise determination of optical constants and sample thickness in terahertz time-domain spectroscopy. *Appl. Opt.* **38**, 409–415. <https://doi.org/10.1364/AO.38.000409> (1999).
50. Hernandez-Cardoso, G. G., Singh, A. K. & Castro-Camus, E. Empirical comparison between effective medium theory models for the dielectric response of biological tissue at terahertz frequencies. *Appl. Opt.* **59**, D6–D11. <https://doi.org/10.1364/AO.382383> (2020).
51. Castro-Camus, E. & Hernandez-Cardoso, G. G. Comparison between effective medium theory models for biological tissues in the THz range. In *2019 44th International Conference on Infrared, Millimeter, and Terahertz Waves (IRMMW-THz)* (2019).
52. Helminiak, J., Alfaro-Gomez, M., Hernandez-Cardoso, G. G., Koch, M. & Castro-Camus, E. Temperature dependence of the dielectric function of dehydrated biological samples in the THz band. *Biomed. Opt. Exp.* **14**, 1472–1479. <https://doi.org/10.1364/BIOE.478787> (2023).

Acknowledgements

J.T. would also like to thank Malina Reitemeyer for her programming support.

Author contributions

J.T., P.A. and R.H. conceived the experiments, J.T. conducted the experiments, O.N. and E.C. developed the basic model idea, J.T. analysed the results and further developed the model with support from G.H. and J.H., J.H. analysed the dry material measurements, A.J. implemented the simplicial homology global optimization algorithm, J.T., M.K., E.C. and P.A. discussed the results and J.T. wrote the manuscript with support from C.M., M.K., E.C. and P.A. All authors reviewed the manuscript.

Funding

Open Access funding enabled and organized by Projekt DEAL. Open access funding enabled and organized by Projekt DEAL and by the Open Access Publishing Fund of Philipps-Universität Marburg. E.C. would like to thank for the support of the Alexander von Humboldt Foundation through an Experienced Researcher Fellowship.

Declarations

Competing interests

The authors declare no competing interests.

Additional information

Supplementary Information The online version contains supplementary material available at <https://doi.org/10.1038/s41598-025-20219-y>.

Correspondence and requests for materials should be addressed to J.T.

Reprints and permissions information is available at www.nature.com/reprints.

Publisher's note Springer Nature remains neutral with regard to jurisdictional claims in published maps and institutional affiliations.

Open Access This article is licensed under a Creative Commons Attribution 4.0 International License, which permits use, sharing, adaptation, distribution and reproduction in any medium or format, as long as you give appropriate credit to the original author(s) and the source, provide a link to the Creative Commons licence, and indicate if changes were made. The images or other third party material in this article are included in the article's Creative Commons licence, unless indicated otherwise in a credit line to the material. If material is not included in the article's Creative Commons licence and your intended use is not permitted by statutory regulation or exceeds the permitted use, you will need to obtain permission directly from the copyright holder. To view a copy of this licence, visit <http://creativecommons.org/licenses/by/4.0/>.

© The Author(s) 2025